Computers and Geotechnics 36 (2009) 1219–1228

Contents lists available at ScienceDirect

Computers and Geotechnics

journal homepage: www.elsevier.com/locate/compgeo

A constitutive model for sand based on non-linear elasticity and the state parameter

D.A. Cameron [a,*], J.P. Carter [b]

[a] University of South Australia, Mawson Lakes Campus, Mawson Lakes, Adelaide, South Australia 5095, Australia
[b] University of Newcastle, New South Wales, Australia

ARTICLE INFO

Article history:
Received 4 August 2006
Received in revised form 9 April 2009
Accepted 14 May 2009
Available online 11 June 2009

Keywords:
Sand
Constitutive model
Triaxial testing
State parameter
Finite element analysis

ABSTRACT

The paper describes the development of a constitutive model for a poorly graded sand, which was used in geotechnical experiments on buried pipes (reported elsewhere). The sand was tested extensively in the laboratory to determine the state parameter constants. Triaxial tests on the sand included conventional drained triaxial compression tests, as well as more specialized shearing tests at constant mean effective stress and others at constant volume. Single element simulation of the triaxial tests was performed to validate the proposed constitutive model. The adopted model allowed non-linear elastic behaviour prior to yielding. After yielding of the sand, the state parameter-based model for the sand permitted non-associated plastic flow. Dilation and frictional strength were both dependent on the current value of the state parameter. The combination of laboratory testing and single element modelling resulted in the selection of a single set of material constants for the soil, which adequately described the full range of triaxial tests. Subsequently the model was applied to the problem of a plate loading test on the sand and the model predictions were compared with the test data.

1. Introduction

A series of full scale soil-structure interaction tests was conducted on uPVC pipes, buried in dry sand, to provide recommendations on the safe cover heights for shallow buried pipe installations subjected to traffic loading. These tests were reported previously in Cameron [1]. The chosen sand was poorly graded and angular, being sand used in the production of concrete. This sand was chosen to represent a poor quality backfill.

Finite element modelling of the buried pipe tests was undertaken to understand the observed non-linear behaviour of the pipe-soil systems. A constitutive model for the sand was required, and after some investigation, a variation of the state parameter model developed by Been and Jefferies [2] was adapted for this purpose. The sand was tested extensively in the laboratory to determine values of the material constants for implementation of the state parameter model.

Triaxial tests on the dry sand included conventional isotropically consolidated and drained tests, with shearing at a constant axial rate of strain, constant mean effective stress shearing tests and constant volume tests. All tests were conducted on samples, nominally 100 mm in diameter and 200 mm high, with initial sample density indices varying between 30% and 80%. Axial strains were taken to 20–25%, in order to approach critical state and to study the dilational behaviour of the sand.

Inspection of the triaxial data revealed non-linear elastic behaviour prior to reaching yield. Therefore the constitutive model included this aspect of the soil's behaviour, along with the observed dilational behaviour.

The emphasis in this work has been on the non-linear behaviour of sand prior to shear yielding and the varying rate of dilatancy once yield has occurred, with ultimately no further dilatancy once the critical state of deformation has been reached. Many existing constitutive models for sands ignore these important effects.

2. Model formulation

The constitutive model for the sand adopted in this study was based on the state parameter concept [2]. The state parameter, ξ, is the difference between the current void ratio of the sand, e, and the void ratio at critical state, e_c, at the same value of mean stress, i.e.:

$$\xi = e - e_c \tag{1}$$

Since the critical state line (or CSL) for sand may be approximated by a straight line in a plot of void ratio against the natural logarithm of mean stress, p', it follows that the state parameter may also be defined as:

$$\xi = e - \Gamma + \lambda_{ss} \ln p' \tag{2}$$

where Γ is the void ratio at a reference mean stress (1 kPa) and λ_{ss} is the slope of the critical state line.

* Corresponding author.
E-mail address: donald.cameron@unisa.edu.au (D.A. Cameron).

0266-352X/$ - see front matter © 2009 Elsevier Ltd. All rights reserved.
doi:10.1016/j.compgeo.2009.05.009

A simple yield criterion was adopted for demarcation between the elastic ($f < 0$) and the elasto-plastic ($f = 0$) phases of soil behaviour:

$$f = q - Mp' = 0 \tag{3}$$

The gradient of the peak strength failure envelope, M, is not constant but varies with the friction angle, ϕ', which in turn varies with the current value of the state parameter.

Collins et al. [3] reviewed Been and Jefferies' data on the variation of friction angle, ϕ', on state parameter and subsequently proposed:

$$\phi' = \phi'_{cv} = A(e^{-\xi} - 1) \tag{4}$$

where A is a material constant and ϕ'_{cv} is the constant volume or critical state, angle of friction.

With this formulation, the current strength of the sand may be evaluated, provided the CSL, the void ratio and effective mean stress are known. Soil dilation may be estimated by adopting Bolton's [4] findings for sand, which suggest that for plane strain conditions:

$$(\phi'_{\max} - \phi'_{cv}) = 0.8\Psi \tag{5}$$

where Ψ is the angle of dilation and $\phi'_{\max}$ is the peak angle of friction.

It may be shown that the rate of dilation, D, for triaxial compression can be expressed by [5]:

$$D = \frac{\delta\varepsilon_p^p}{\delta\varepsilon_q^p} = \frac{-6\sin\Psi}{(3 - \sin\Psi)} \tag{6}$$

This equation is essentially a flow rule for yield behaviour of the sand. The angle of dilation provides the rate of change, D, of plastic volumetric strain ($\delta\varepsilon_p^p$) with change of plastic deviatoric strain ($\delta\varepsilon_q^p$).

The non-linear elasticity of sand was incorporated by reviewing research into changes in shear modulus with void ratio and stress state. It has been proposed [6] that the current secant shear modulus, G_s, depends on the soil constants, f and g, as well as the ratio of the current shear stress, τ, to the peak shear stress, $\tau_{\max}$, in the plane strain formulation:

$$\frac{G_s}{G_o} = 1 - f\left(\frac{\tau}{\tau_{\max}}\right)^g \tag{7}$$

where G_o is the small strain shear modulus.

The small strain shear modulus was assumed to be a function of both the initial void ratio, e_o, and the current effective mean stress, after [7]:

$$G_o = C_g\left(\frac{(e_g - e_o)^2}{1 + e_o}\right)(p_a)^{(1-n_g)(p')^{n_g}} \tag{8}$$

where C_g, n_g and e_g, are material constants, e_o the initial void ratio and p_a is the atmospheric pressure.

A tangent shear modulus, G_t, for plane strain may be derived by differentiating Eq. (7) [8], which resulted in the following equation:

$$\frac{G_t}{G_o} = \frac{(G_s/G_o)^2}{\left[1 - f(1-g)\left(\frac{\tau}{\tau_{\max}}\right)^g\right]} \tag{9}$$

The generalisation of Eq. (9) to three-dimensions was made, based partly on [9] and by analogy. The resultant expression after differentiation to determine the tangent shear modulus was:

$$\frac{G_t}{G_o} = \frac{(G_s/G_o)}{\left[1 - f(1 - g\left(\frac{\sqrt{J_2}}{\sqrt{J_{2\max}}} - \frac{\sqrt{J_{2o}}}{\sqrt{J_{2o}}}\right)\right]} \tag{10}$$

where $J_2 = 1/6\left[(\sigma'_1 - \sigma'_2)^2 + (\sigma'_2 - \sigma'_3)^2 + (\sigma'_1 - \sigma'_3)^2\right]$ is the deviatoric stress invariant, J_{2o} the value of J_2 at the commencement of monotonic loading, $J_{2\max}$ the maximum value of J_2 attainable at the current effective mean stress, p', corresponding to the failure criterion (Eq. (6)).

The tangent bulk modulus, K_t, was allowed to increase as a power law function of mean effective stress [9,10], given by:

$$K_t = D_s(p')^{n_k}(p_a)^{(1-n_k)} \tag{11}$$

where D_s and n_k are considered to be material constants.

Since G_t and K_t, are both independently formulated, conservative elasticity is not guaranteed. Therefore, Poisson's ratio varies in this model with the elastic moduli.

In order to achieve realistic modelling of soil behaviour, it was found necessary to place a lower limit on G_t relative to G_o, which reduced with increasing deviator stress. This requires the introduction of a further material constant, r_g, the ratio of the minimum value of G_t and G_o, which could vary between zero and unity. If r_g is zero, there is no limit on the reduction of G_t with deviator stress. However if r_g is unity, there is no reduction in G_t with deviator stress.

It is noted that in the proposed model the elastic domain is not closed on the hydrostatic axis, which implies, for example, that oedometric behaviour of the sand must be perfectly elastic. This is an acknowledged shortcoming of this model for some stress paths. However, the stress paths of interest in the studies considered here and elsewhere by the authors, i.e., triaxial shearing and the behaviour of backfill sand around embedded pipes subject to surface loading, involves predominantly shear loading. For these stress paths the model is capable of providing reasonable predictions, as will be demonstrated.

The equations presented above are the basis for the constitutive model of sand with a non-linear, elasto-plastic stress–strain law and post-yield dilation, with non-associated flow. This combination of non-linear elasticity and a variable rate of plastic dilation, culminating in no further dilation at the critical state, is a defining feature of this unique constitutive model for sand.

The model requires values for 12 material constants, namely: λ, Γ, A, ϕ_c, D_s, n_k, C_g, e_g, n_g, f, g and r_g. The following sections outline how these values were determined for the sand.

3. Description of the sand

The sand was angular, poorly graded and was composed of 97% quartz, 1% muscovite, 1% feldspar and 1% tourmaline and iron

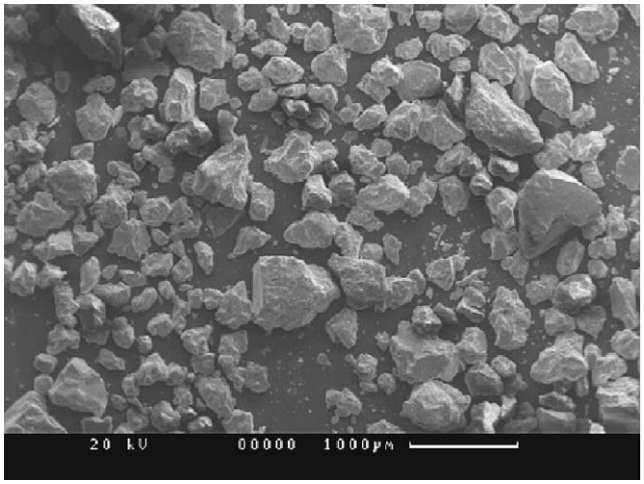

Fig. 1. Scanning electron microscope image of the sand.

oxides. The angularity of the sand is clearly evident in the scanning electron microscope slide shown in Fig. 1.

Key particle sizes, D_{10} and D_{60}, were 0.16 and 0.41 mm, respectively. The sand had a uniformity coefficient of 2.6 and a coefficient of curvature of 0.92. The particle density was 2.66 t/m^3 and the maximum and minimum densities were 1.75 and 1.405 t/m^3, respectively. The maximum and minimum void ratios were 0.893 and 0.520, respectively.

4. Triaxial testing procedure

A series of triaxial tests was conducted to evaluate the state parameter material constants. The series included conventional triaxial tests and both constant mean stress and constant volume tests. All samples were tested dry and the test samples were prepared to density indices ranging between 30% and 80%. Most of the tests were conducted on samples compacted to a medium dense state, reflecting the general level of compaction achieved with the backfill in the buried pipe experiments. Large axial strains were achieved, usually between 20% and 25%, in order to approach critical state.

Samples were set up at the desired dry density by clamping a split tube former over the bottom pedestal and applying a small vacuum pressure to hold the sample membrane to the inside of the former. The soil was placed in layers, which were rodded uniformly to achieve the desired sample height for the required density. After securing the sample a vacuum pressure of 10–15 kPa was transferred to the sample through the drainage port to maintain its shape while the former was removed. An example of a ready-to-test dry sand specimen is provided in Fig. 2.

Although lubricated and over-sized platens have been advocated to ensure uniform sample stresses [10], conventional platens were used. This decision was based on practicality and the adoption of a length to diameter ratio of the sample, which was sufficiently large to minimise this problem [11]. All samples were approximately 100 mm in diameter and 190 mm high and so had a length to diameter ratio of 1.9.

A membrane thickness of 0.35 mm was found to be the practical minimum thickness for this sand to ensure leaks did not occur at the large sample strains attained in the tests. The influence of the membrane on the soil response was considered [12], but was estimated to be negligible.

Samples were isotropically consolidated at the rate of 2.5 kPa/min before commencing sample shearing at a strain rate of no more than 0.05 mm/min. The initial consolidation settlement was relatively small and was assumed to be isotropic. Volume changes were estimated from cell fluid volume changes (de-aired water), which were measured by a GDS hydraulic ram system. Volumes were corrected for cell volume changes in response to cell pressure changes and for the penetration of the loading ram. Axial strains were measured electronically outside the cell, while axial load was measured inside the cell.

Samples were noticeably barrelled at the end of testing as indicated in the photographic example on the right-hand side of Fig. 2.

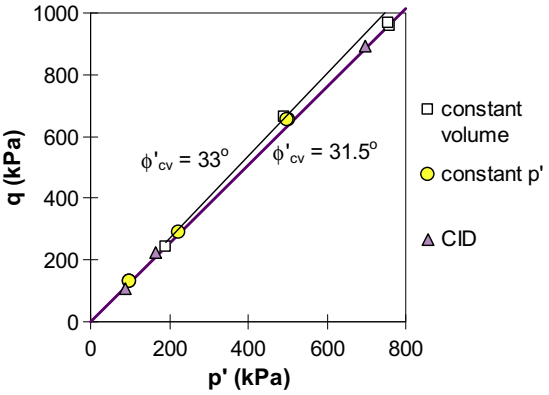

Fig. 3. Critical state strength (ϕ'_{cv}) estimated from stress state at end of triaxial tests.

5. Test results

5.1. Strength of the sand

The peak friction angle was found to increase almost linearly with density index. The critical state shear strength, ϕ'_{cv}, was estimated from the triaxial data (refer Fig. 3) to be 31.5°.

5.2. The critical state line

It was found that the interpreted position of the critical state line (CSL) varied slightly between the different types of tests, as indicated in Fig. 4. However, as is often the case with triaxial tests on sand, particularly for dense samples, interpretation of the end point of each test (critical state) is problematic because localised

Fig. 2. An example of a prepared dry sand sample and deformed shape after testing.

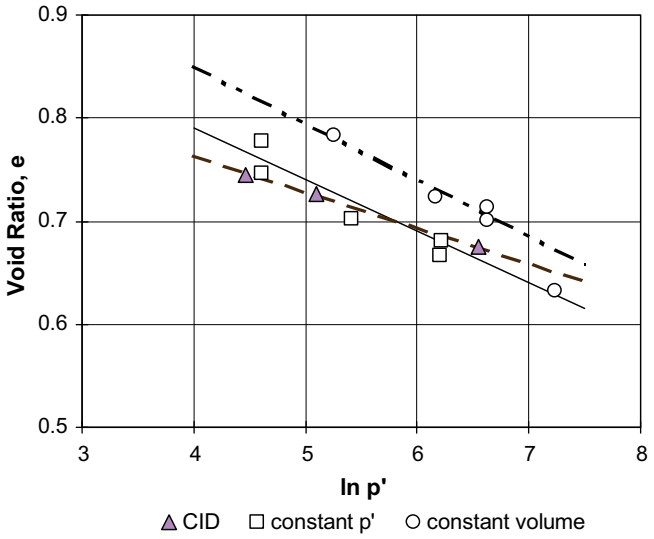

Fig. 4. Variation of CSL with type of triaxial test.

deformations (shear bands) can occur, i.e., homogeneous deformation is not always achieved. The chosen CSL was based on the constant volume tests as it gave lower positive values of $(\phi'_{max} - \phi'_{cv})$ at a state parameter near zero than either of the other two alternatives. Theoretically ϕ'_{max} must equal (ϕ'_{cv}) at critical state, i.e., when the state parameter is zero. The critical state line was defined by values of Γ of 1.07 and λ of 0.055. Material constant, A, was found to be 0.98 (refer Fig. 5 and Eq. (4)).

5.3. Dilation of the sand

Bolton [4] recommended that dilation, expressed as the rate of change of total volumetric strain to change in total axial strain, could be estimated by $-0.3I_R$, where I_R is a dilation index. The recommendation was found to be appropriate for this sand, provided the dilation index, I_R, was expressed in terms of the density index of the sand, I_D, as follows:

$$I_R = I_D(Q - \ln p') - 1 = I_D(9 - \ln p') - 1 \quad (12)$$

Bolton's dilatancy index was formulated originally with a value of Q of 10. However, he had anticipated that lower values of Q might be appropriate for more angular sands.

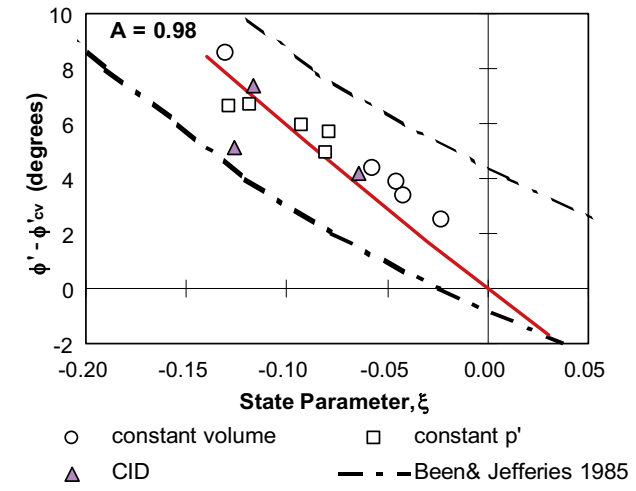

Fig. 5. $(\phi'_{max} - \phi'_{cv})$ as a function of state parameter, ξ.

It was found from the triaxial data that the dilation index was directly proportional to the state parameter:

$$I_R = -10.7\xi \quad (13)$$

Bolton recommended that the effective strength difference $((\phi'_{max} - \phi'_{cv})$ in degrees could be approximated by $5I_R$ for plane strain conditions and $3I_R$ for triaxial conditions. For this sand, Bolton's equation for plane strain proved to be a reasonable approximation to the triaxial compression data. Indeed better estimates were possible with a slightly higher multiplier of 5.6 on the dilation index.

Bolton also recommended that the effective strength difference for plane strain could be approximated by 0.8ψ. This relationship has been applied to triaxial conditions by numerous researchers. Using Eq. (6), the maximum dilation angle for triaxial conditions, Ψ_{max}, was derived from the triaxial data and compared with $(\phi'_{max} - \phi'_{cv})$. These data have been plotted in Fig. 6. Three of the five "constant volume" tests have been included in this plot as

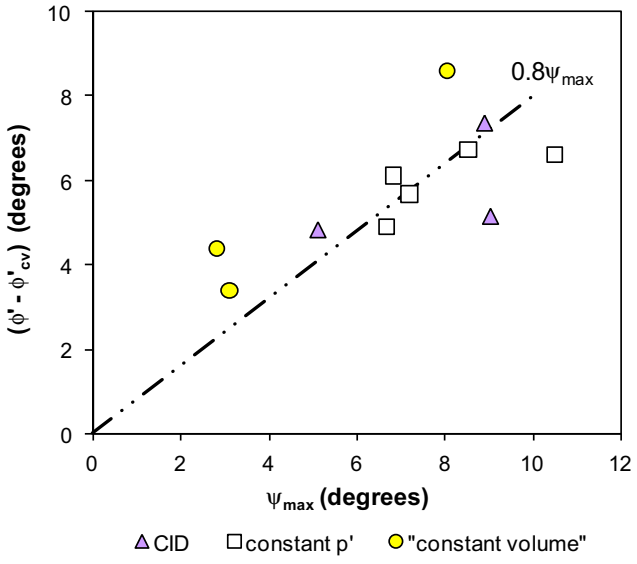

Fig. 6. $(\phi'_{max} - \phi'_{cv})$ as a function of maximum angle of dilation, from Eq. (6).

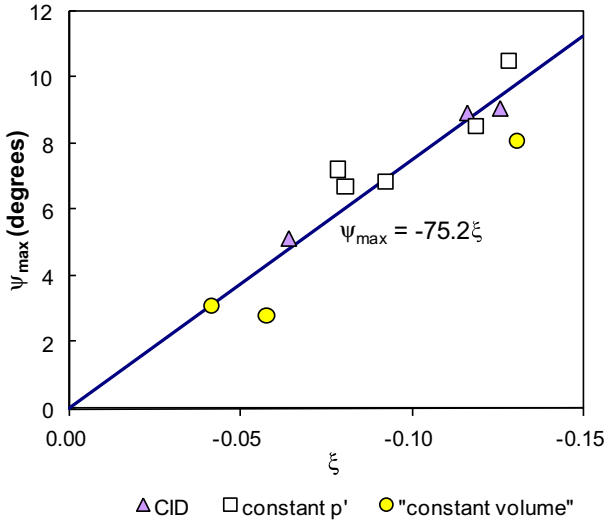

Fig. 7. The variation of maximum angle of dilation with state parameter.

the cell deformation correction had been programed incorrectly, allowing some dilation during testing. The legend in Fig. 6 highlights these tests as imperfect "constant volume" tests.

Bolton's linear relationship has been plotted in Fig. 6 and although the line passes through the data, a poor correlation was evident. Although the line of best fit for the data had a gradient of almost 0.8 (0.79), the correlation coefficient was just 0.14.

Stronger correlations were found for linear relationships between the estimated maximum dilation angle and both I_R and ξ (with correlation coefficients of 0.80 and 0.85, respectively). The plot of dilation angle against state parameter is provided in Fig. 7. The two relationships were:

$$\psi_{max} = 7.09 I_R \text{ degrees} \quad (14)$$

$$\psi_{max} = -75.2 \xi \text{ degrees} \quad (15)$$

Eq. (15) is attractive in its simplicity, and suggests that state parameter and the flow rule may provide the basis of a powerful model for the stress-deformation behaviour of sand. This issue probably requires further investigation but is not pursued further in this paper.

6. Parameter values

The critical state friction angle, ϕ'_{cv}, CSL and material constant, A (Eq. (4)) were presented in the previous section, thus accounting for four of the twelve material constants required by the model. The remaining model constants were determined by curve fitting the stress–strain and dilational behaviour of the sand as revealed from the triaxial testing. No systematic method of curve fitting was pursued in this study – the so-called "best fit" predictions of the experimental data were determined merely by inspection. A single element model was developed in a spreadsheet and subsequently the model predictions were compared with the triaxial test results to evaluate the remaining soil material constants.

6.1. Comparison between model predictions and test data

The selection of model parameters was based on the degree of fit of the model output to the variation of both stress ratio (q/p') and volumetric strain, with axial strain. Chosen values of the material constants are provided in Table 1. The comparisons of the triaxial test data with the model employing these material constants are provided in Figs. 8–10, for the three sets of triaxial data. The initial density index of the sand is indicated on each plot.

The comparisons provided in the stress–strain and volumetric strain–axial strain plots are remarkably good for the majority of tests, although the predicted transition from elastic to elasto-plastic behaviour was relatively abrupt, and the peak stress therefore tended to be overestimated. It is worth noting that the pressure and density dependent behaviour of this sand has been captured well over the ranges investigated (mean stress from approximately 50–800 kPa and density index from 30% to 80%) using only a single set of model parameters. This observation reinforces the potential of the model, which is based on pressure-dependent, non-linear elasticity and the state parameter concept.

7. Finite element modelling

The state parameter model was implemented in finite element program, AFENA [13]. In order to validate the implementation, single finite element analyses of the conventional triaxial tests were performed, and the predictions were compared with the single element results from the spreadsheet. Axi-symmetric analyses were conducted with a single eight-noded quadrilateral element, having nine Gauss points, representing a quarter of the triaxial specimen. Appropriate boundary conditions were applied to the finite element model.

Table 1
Values of material constants from the single element model.

λ	Γ	A	ϕ_c (°)	D_s	n_k	C_g	e_g	n_g	f	g	r_g
0.055	1.07	0.98	31.5	200	0.5	300	2.3	0.5	0.99	0.2	0.03

Good comparisons were obtained between the test data, the single element method and the AFENA finite element analyses (FEA). It is worth noting that singularities at the triaxial stress condition and subsequent difficulties with stress integration in the finite element analyses can occur at low mean stresses and at the sharp corners of the Mohr–Coulomb failure envelope in the π plane of stress space. In order to avoid these difficulties, the apex of the Mohr–Coulomb line was approximated with a hyperbola and the corners were rounded using circular arcs, in accordance with [14].

7.1. Application to plate loading tests

The stiffness of the compacted dry sand was evaluated by two simple, plate loading tests on the surface of the sand, while the sand was contained within a cylindrical steel drum. The diameter of the loading plate was 270 mm. The steel drum was 1.15 m high and had an internal diameter of 565 mm. The density index of the soil was 75% on average, found by weighing the sand in the drum.

The soil was modelled with 440, 15-noded triangular elements, each element having 12 Gauss points. The axi-symmetric mesh is depicted in Fig. 11. Boundary conditions are illustrated for a mesh with an interface joint between the sand and the steel drum. The joint was removed and the appropriate boundary displacement conditions were applied, when either perfectly rough or perfectly smooth conditions were adopted at the sidewall. For the smooth wall case, vertical fixity was required along the base, while horizontal displacements were constrained at either side boundary. For the perfectly rough wall model, the vertical displacement was also constrained along the outer surface.

Prior to applying load to the plate, an arbitrary average initial stress state was applied throughout the soil mass, consisting of 10 kPa, vertically and 4 kPa, horizontally. A non-zero initial stress state was necessary to initiate the analysis because of the stress-dependence of the material behaviour. The assumed small initial stresses should have had minimal effect on the predictions, since the stress field in the soil soon becomes dominated by the applied surface loading.

Loading through the rigid plate was simulated by enforced incremental displacements of the 21 surface nodes over the radius of the plate. The load on the plate at a particular displacement was determined by summation of the reactions at these same nodes. The displacement increments were typically 0.005 mm. These small size steps were found necessary to provide reasonable numerical stability of the finite element analyses.

The joint at the sidewall was a Goodman type, elasto-plastic interface element, which required elastic shear stiffness, a normal stiffness, and an effective angle of interface friction. The joint interface was assumed to be non-cohesive and non-dilatant. A series of direct shear box tests of an interface were conducted to provide joint parameters. Subsequently, the values adopted for the joint stiffness were 1.0×10^4 kPa/m for the shear stiffness and 1.0×10^7 kPa/m for the normal stiffness. The joint strength was defined by an angle of friction of 25°.

7.2. Soil variables

A series of Mohr–Coulomb analyses was first attempted, which did not include the state parameter concept. A wide range of

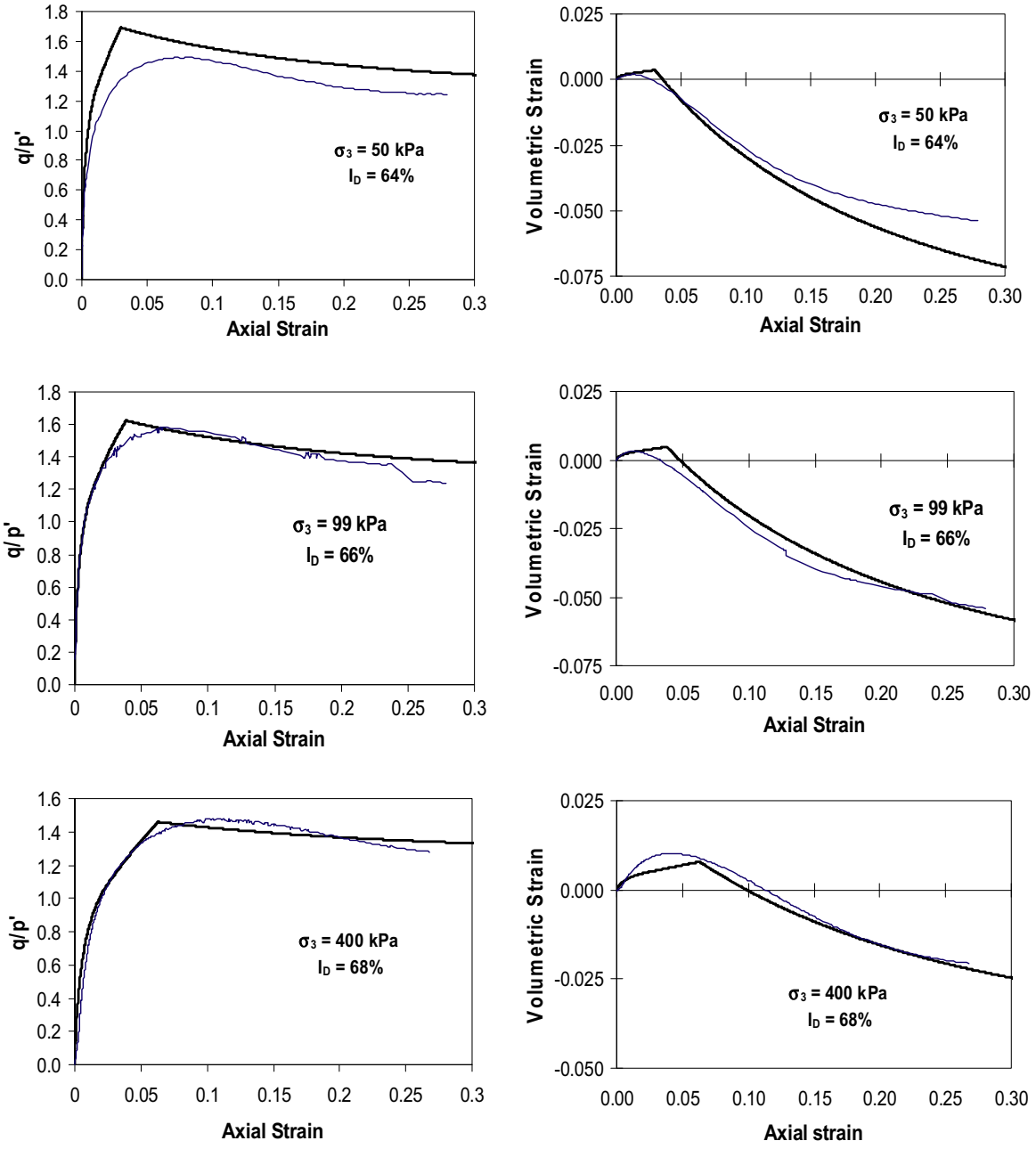

Fig. 8. Comparison of single element model and test data – conventional triaxial tests.

effective friction angles and angles of dilation were trialed, in an attempt to match the experimental data. The sidewall boundary was treated as either perfectly smooth or perfectly rough.

For the state parameter FEA runs, the soil density index was assumed to be 50%, 75% or 85%. Density indices were converted to initial void ratios on the basis of the maximum and minimum void ratios for the sand. In this series of analyses, usually a joint was incorporated at the sidewall.

7.3. FEA results

Upon review of the results of the Mohr–Coulomb analyses, it was found that as the strength and dilation of the sand were increased, the stiffness of the soil to the surface loading also increased. A rough wall condition gave a significantly stiffer footing response than the comparable smooth wall case. Nonetheless, the experimental data could not be matched, even after unrealistically adopting a peak effective friction angle of 50° and a dilation angle equal to the friction angle. The initial stiffness predicted by the Mohr–Coulomb model was substantially less than that of the sand as revealed in the plate load tests. Up to a plate deflection of 1 mm, the predicted stiffness was approximately 30% of the stiffness derived from the test.

The state parameter model was considerably more successful at predicting the stiffness of the plate-soil system. The load–deflection plots for the three assumed initial density indices are provided in Fig. 12. In all these analyses, an interface joint was incorporated along the sidewall. Very few analyses achieved the target plate displacement of 10 mm. Some finite element analyses ended prematurely after the development of tension in Gauss points near the singularity at the edge of the loading plate and close to the soil surface.

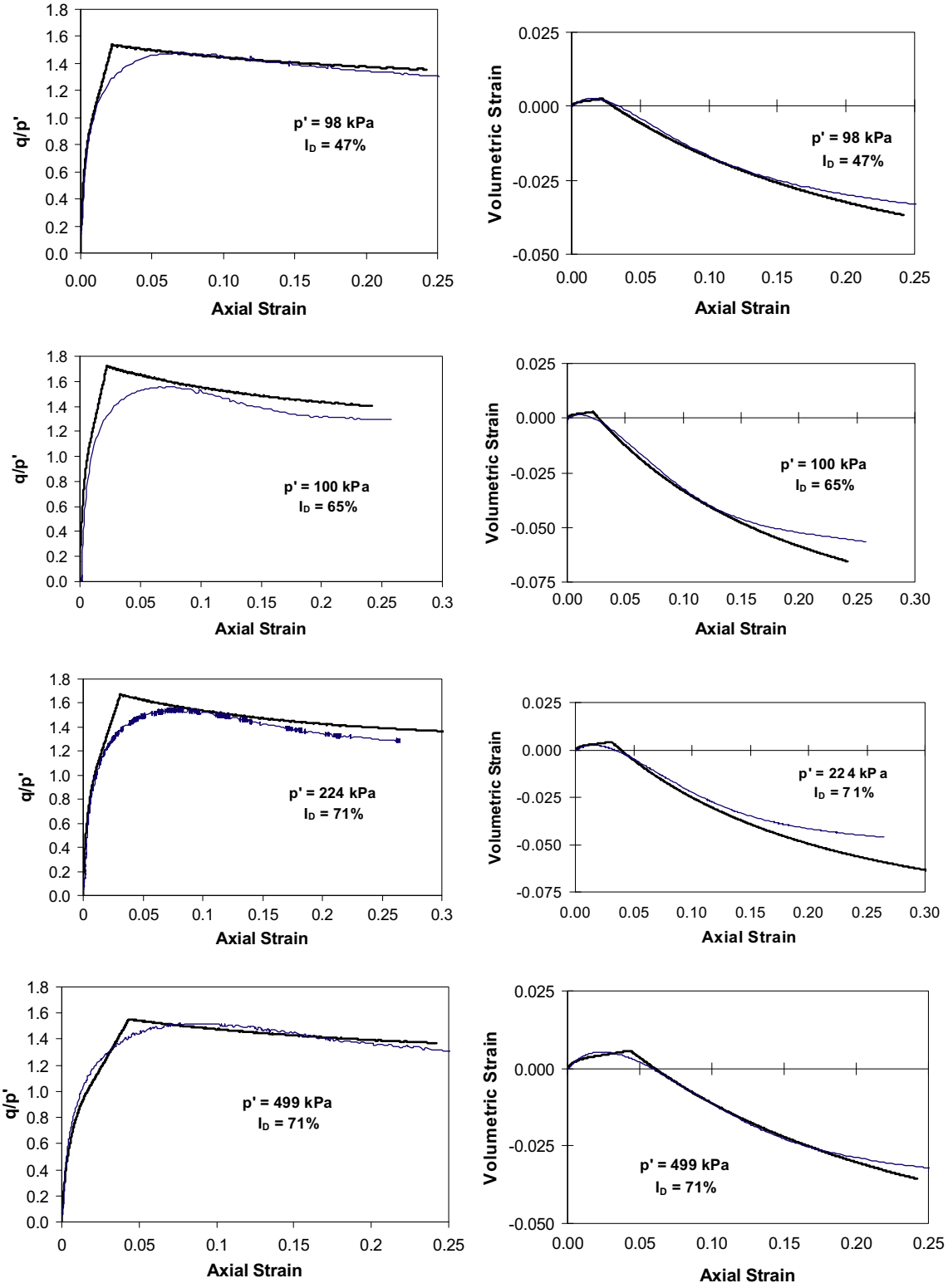

Fig. 9. Comparison of single element model and test data – constant mean stress tests.

It is apparent that a sand density index, I_D, of 85% brought the finite element analysis in line with the experimental data. As the density index decreased, the modelled sand response was less stiff. The density index determines the soil's initial void ratio and, with the effective mean stress, determines the state parameter, which impacts directly on the peak friction angle and dilation of the soil, as well as the soil stiffness.

The influence of the frictional resistance at the side-wall on the soil response was then examined by running finite element analyses with a sand I_D of 85% and with either perfectly rough, or

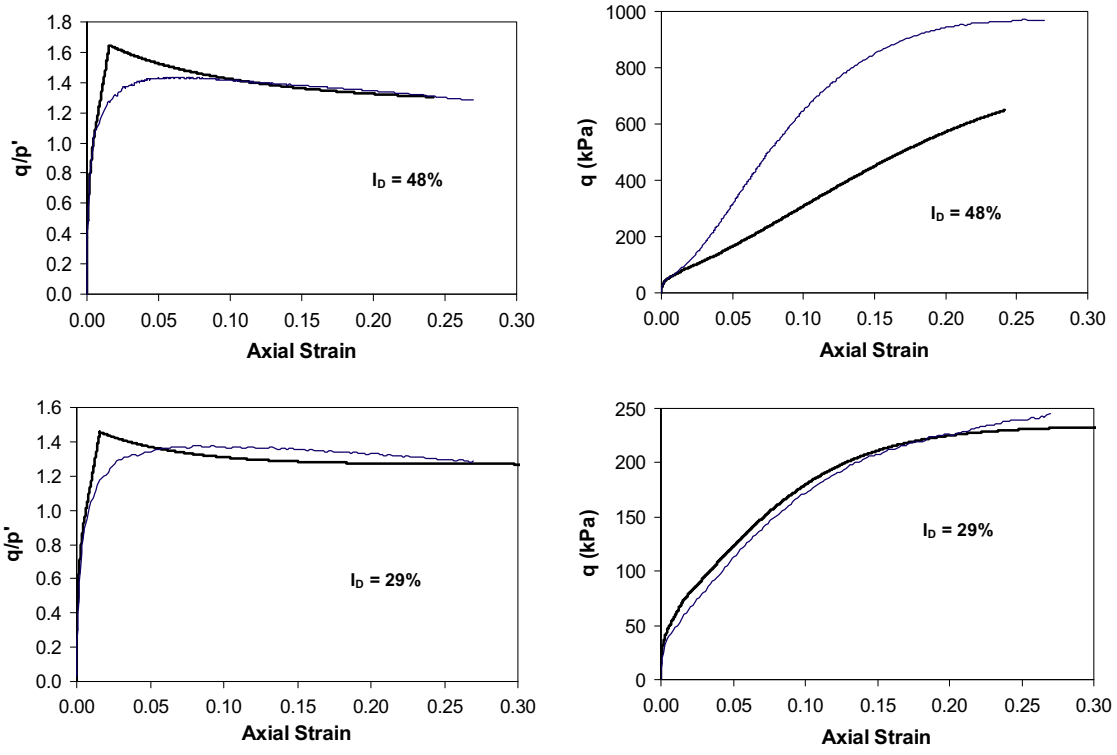

Fig. 10. Comparison of single element model and test data – constant volume tests.

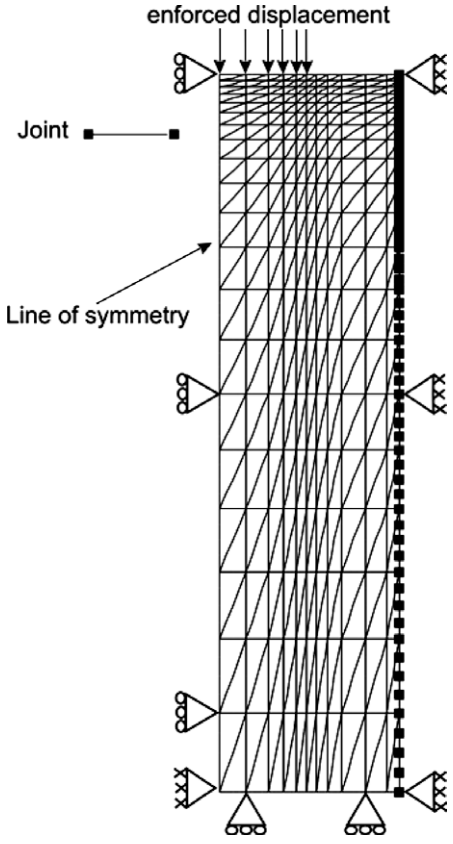

Fig. 11. The mesh for FE analysis of the plate loading test (scale in metres).

perfectly smooth, walls. It was observed that the jointed wall model resulted in a load–deflection curve that was slightly less stiff

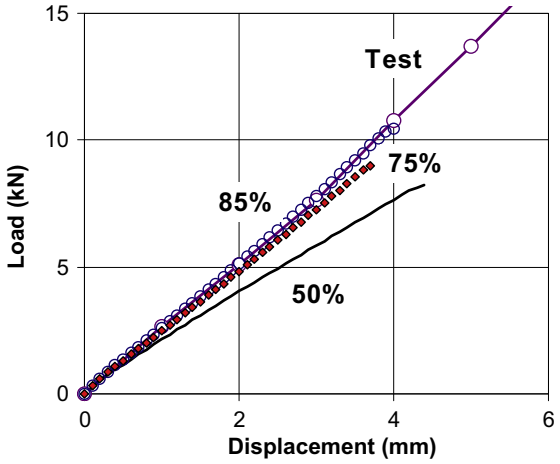

Fig. 12. State parameter finite element analysis outputs with Goodman joint at sidewall and variable initial soil density index.

than the response of the rough wall analysis. In contrast the output from the smooth wall case indicated significantly less initial stiffness, approximately 30% less up to a plate displacement of 2 mm.

Output from the most successful FEA (soil I_D = 85% and a Goodman joint included) at a plate displacement of 4 mm is provided in Figs. 13 and 14. Fig. 13 provides contours of the vertical deflections of the sand. Very little deformation was evident in the lower half of the mesh. While the plate had pushed down the underlying sand surface uniformly by 4 mm, the adjacent sand surface had settled only by 1 mm. Fig. 14 indicates the locations of plastic Gauss points. Yield had extended beside the edge of the plate to a depth of 0.4D, approximately, where D is the plate diameter. All surface elements outside the loaded area had yielded as well as the elements along the sidewall within a depth of 0.1D. Yield in this zone was anticipated as the stress levels are low near a free surface.

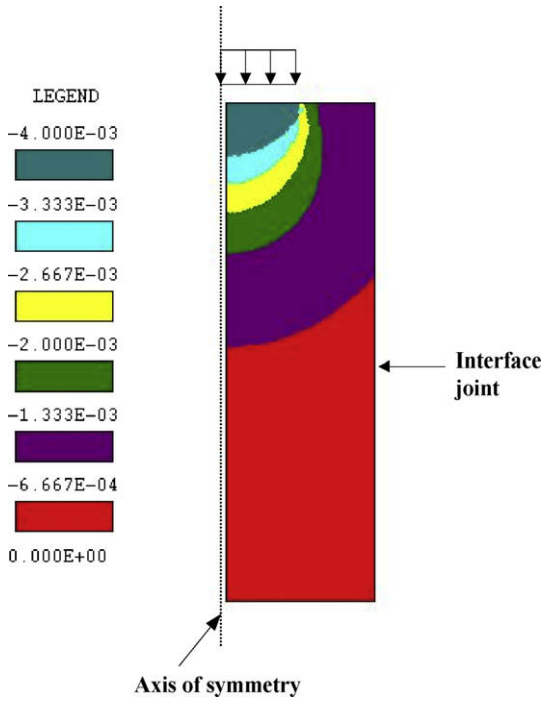

Fig. 13. Vertical deformations (in metres) of the sand under plate loading from FEA analysis (plate displacement of 4 mm).

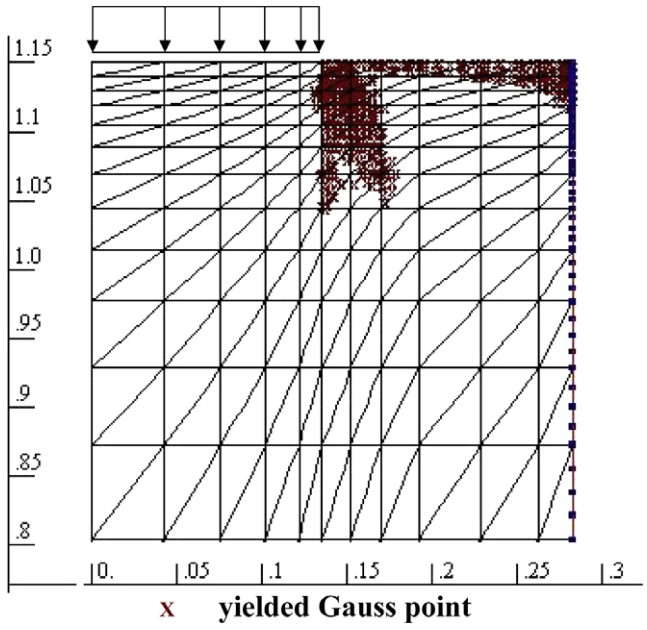

Fig. 14. Yield locations within the top of the mesh (plate displacement of 4 mm).

8. Summary and findings

The major findings of the triaxial testing program were;

(a) The critical state shear strength parameter for the sand, ϕ'_{cv}, was estimated to be 31.5°.
(b) The position of the critical state line in $e - \ln p'$ space varied slightly between the different types of tests, with the constant volume tests providing a "higher" CSL, defined by values of Γ of 1.07 and λ of 0.055.
(c) The material constant A [3] required to define the relationship between $(\phi' - \phi'_{cv})$ and state parameter, ξ, was determined to be 0.98.
(d) Bolton's dilatancy index [4] was formulated with Q being equal to 9, rather than 10, for the angular sand in this study.
(e) Bolton's dilatancy index [4] was found to be directly proportional to the negative of the state parameter, i.e., $I_R = -10.7\ \xi$.
(f) The recommendation of $(\phi'_{max} - \phi'_{cv}) = 3I_R$ for a triaxial stress state [4] was found to greatly underestimate the difference in shear strength angles for this sand. Interestingly, Bolton's equation for plane strain $(\phi'_{max} - \phi'_{cv}) = 5I_R$ was a better approximation to the triaxial compression data.
(g) The flow rule for triaxial conditions, when applied to the experimental data, yielded estimates of dilation angle (ψ_{max}) which were found to correlate well against both Bolton's dilation index and state parameter. The state parameter correlation was found to be slightly stronger. The dilation angle in degrees can be approximated by multiplying ξ by a factor of -75.

From a review of the soil behaviour, an elasto-plastic, isotropic model incorporating the state parameter concept has been developed. Yield was defined by the Mohr–Coulomb criteria. Deformations during yielding are based on a non-associated flow rule defined by Bolton's findings and the state parameter concept.

The application of a spreadsheet for single element modelling of triaxial test data was shown to be valuable for developing soil constitutive models and evaluating material constants. The single element model incorporated non-linear elasticity with the shear and bulk modulus not directly linked. The non-linearity requires eight material constants. A set of material constants was established, which adequately modelled the majority of the triaxial tests on the sand. Subsequently the model was incorporated into finite element program AFENA. The single element analyses of the conventional triaxial tests were found to compare favourably with the finite element predictions of the same tests, thus validating both implementations of the model.

The state parameter model was then applied to the numerical modelling of a plate loading test in the sand, confined within a drum. This geotechnical problem is difficult to model because of the stress singularity at the edge of the rigid loading plate and the likelihood of tension and plastic yielding near the unloaded soil surface. It was observed that the state parameter model was superior to the simpler Mohr–Coulomb model, in which a constant effective angle of friction and angle of dilation are assumed. The state parameter model constantly updates values of both dilation and angle of friction based on the current effective stress and void ratio of the soil, i.e., based on the value of the state parameter.

The implementation of an interface joint along the sidewall improved the modelling of the plate load test with the state parameter, when compared with the assumption of a perfectly rough sidewall condition. In contrast, a perfectly smooth wall was found unable to represent the test data adequately.

The average density index of the soil in the plate loading tests was estimated to be 75%, however a density index of 85% was required in the finite element analyses to achieve the best match with the load–deflection test data. It could be concluded that the average density index was underestimated or the proposed soil model may need further improvement.

References

[1] Cameron DA. 2005. Analysis of Buried Flexible Pipes in Granular Backfill Subjected to Construction Traffic. Ph.D. Thesis, The University of Sydney.

[2] Been K, Jefferies MG. A state parameter for sands. Géotechnique 1985;35(2):99–112.
[3] Collins IF, Pender MJ, Yan W. Cavity expansion in sands under drained loading conditions. Int J Num Anal Methods Geomech 1992;16(1):3–23.
[4] Bolton MD. The strength and dilatancy of sands. Géotechnique 1986;36(1):65–78.
[5] Carter JP, Booker JR, Yeung SK. Cavity Expansion in Cohesive Frictional Soils. Géotechnique 1986;36(3):349–58.
[6] Fahey M, Carter JP. A finite element study of the pressure meter test in sand using a nonlinear elastic plastic model. Can Geotech J 1993;30:348–62.
[7] Hardin BO, Black WL. Sand stiffness under various triaxial stresses. J Soil Mech Found Eng ASCE 1966;92(SM2):27–42.
[8] Lee J, Salgado R. Analysis of calibration chamber plate load tests. Can Geotechn J 2000;37:14–25.
[9] Naylor DJ, Pande GN, Simpson B, Tabb R. Finite elements in geotechnical engineering. Swansea, Wales, UK: Pineridge Press; 1981.
[10] Lo SCR, Lee IK. Response of Granular Soil along Constant Stress Increment Ratio Path. ASCE J Geotech Eng 1990;116(3):355–76. March.
[11] Bishop AW, Green GE. The influence of end restraint on the compression strength of a cohesionless soil. Géotechnique 1965;15(3):243–66.
[12] Ooi JY. 1990. Bulk Solids Behaviour and Silo Wall Pressures. Ph.D. Thesis, University of Sydney, School of Civil and Mining Engineering.
[13] Carter JP, Balaam NP. AFENA – a general finite element program for geotechnical engineering school of civil and mining engineering. Sydney, Australia: University of Sydney; 1995.
[14] Abbo AJ, Sloan SW. A smooth hyperbolic approximation to the Mohr–Coulomb yield criterion. Comput Struct 1995;54(3):427–41.